# Oversampling requirements for pixelated-imager systems

**Ofer Hadar,** MEMBER SPIE
Ben-Gurion University of the Negev
Department of Electrical and
Computer Engineering
P.O. Box 653
84105 Beer-Sheva, Israel

**Glenn D. Boreman,** MEMBER SPIE
University of Central Florida–CREOL
P.O. Box 162700
Orlando, Florida 32816-2700
E-mail: boreman@creol.ucf.edu

**Abstract.** The image quality resulting from a 2-D image-sampling process by an array of pixels is described. The description is based on a Fourier transformation of the Wigner-Seitz cell, which transforms a unit cell of the sampling lattice in the spatial domain into a bandwidth cell in the spatial-frequency domain. The area of the resulting bandwidth cell is a quantitative measure of the image fidelity of the sampling process. We compare the image-quality benefits of three different oversampling geometries in terms of the modulation transfer function (MTF) as a function of the amount of oversampling used.  [S0091-3286(99)00205-6]

Subject terms: image quality; modulation transfer functions; oversampling.

Paper SIS-03 received July 14, 1998; revised manuscript received Aug. 13, 1998; accepted for publication Aug. 13, 1998.

## 1 Introduction and Motivation

The spatial sampling rate of the detector array is an important parameter in pixelated-imager systems. Focal-plane arrays (FPAs) are being developed with ever increasing numbers of pixels. In the infrared (IR) portion of the spectrum, the need to develop scene-projection (SP) systems capable of characterizing the performance of these high-quality imagers has resulted in steadily increasing requirements for the test equipment. An IRSP system must be designed to test a number of different imager systems with various pixel formats and fields of view. Thus, it is not feasible to expect that the ideal situation of a pixel registered one-to-one match between the IRSP and the IRFPA will be possible in general, even assuming a continuous zoom magnification of the projector. Hence, it is desirable to oversample the imager under test, that is, to project a higher number of pixels than the imager can resolve. It is intuitive that an IRSP system with a large number of pixels can approximate a continuous scene more accurately than a system with fewer pixels. Because the number of independent pixels in an IRSP is an important cost driver, however, it is of interest to quantify the incremental image-quality benefits that can be expected from a given amount of oversampling. We have developed a procedure that enables IRSP pixel-count specifications to be developed as a tradeoff between performance and cost, using an image-quality metric based on the area of the bandwidth cell in the spatial-frequency domain. The bandwidth cell is the Fourier transform of the unit cell of the sampling lattice in the spatial domain.

## 2 Sampling MTF

Sampling by a 2-D array of finite-sized pixels involves two distinct modulation transfer function (MTF) contributions: one for the sampling process associated with the finite spacing between samples and one for the spatial averaging process associated with the finite size of the pixels. We assume that these two MTFs multiply to yield an aggregate MTF for the sampling-and-averaging process. Validity of the multiplication of MTFs depends on assumptions of linearity and shift invariance. Shift invariance does not apply to pixelated-imager systems, and it is necessary to define[1] a shift-invariant sampling MTF as an ensemble average over all possible positions of the scene with respect to the sampling locations.

The MTF contribution of image averaging over pixels of finite dimension is well known. For a 1-D rectangular pixel, the pixel MTF is a sinc function

$$\mathrm{MTF}(\xi)_{\mathrm{pixel}} = \mathrm{sinc}\,(p\xi) \equiv \frac{\sin(p\xi\pi)}{p\xi\pi}, \tag{1}$$

where $\xi$ is the image spatial frequency, and $p$ the full width of the pixel. Square pixels are the most common shape in practice, but others are possible such as hexagonal[2] or tapered,[3] for which the pixel MTF is inherently a nonseparable 2-D function. The pixel MTF in Eq. (1) does not take into account the effect of the pixel spacing on image quality. We previously derived[4] the sampling MTF using a statistical treatment of the intensity sampled by an array of pixels. The sampling MTF can also be expressed as a sinc function,

$$\mathrm{MTF}(\xi)_{\mathrm{samp}} = \mathrm{sinc}\,(\Delta\xi), \tag{2}$$

where $\Delta$ is the distance between the samples. The overall sampling-and-averaging MTF is given by multiplication of these two functions,

$$\begin{aligned}\mathrm{MTF}(\xi)_{\mathrm{total}} &\equiv \mathrm{MTF}(\xi)_{\mathrm{pixel}} \times \mathrm{MTF}(\xi)_{\mathrm{samp}} \\ &= \mathrm{sinc}\,(p\xi) \times \mathrm{sinc}\,(\Delta\xi).\end{aligned} \tag{3}$$

Equation (3) shows that two parameters determine the quality of the sampled image: the pixel size $p$ and the distance $\Delta$ between the pixels in the array. Decreasing the dimensions of either of these parameters will improve the

 0091-3286/99/$10.00 

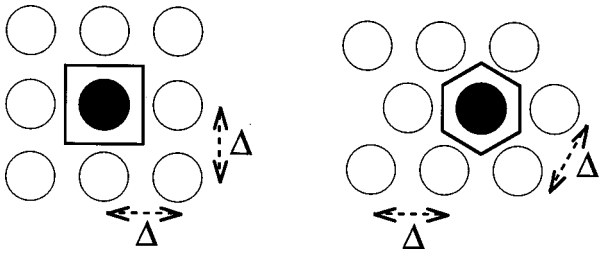


**Fig. 1** WS cell for a square lattice and a hexagonal lattice.

image quality. In the limit of $p$ and $\Delta$ going to zero, the sampling-and-averaging MTF approaches unity, because the sampled signal approaches a continuous one. A similar analysis can be applied for the case of a 2-D sampling lattice, where the pixel width $p$ is replaced by the normalized pixel function $p(\mathbf{x})$

$$p(\mathbf{x})=\begin{Bmatrix} 1/A_p, & \text{for } \mathbf{x} \text{ inside the pixel} \\ 0, & \text{for } \mathbf{x} \text{ outside the pixel} \end{Bmatrix}, \tag{4}$$

where $A_p$ is the area of the pixel and $\mathbf{x}$ is the 2-D position vector. Similarly, the sample spacing $\Delta$ is replaced by the Wigner-Seitz cell, defined[5] as the region of space surrounding a sample point that is closer to that point than to any other. We define Wigner-Seitz (WS) function $w(\mathbf{x})$, normalized with respect to the area of the WS cell $A_w$:

$$w(\mathbf{x})=\begin{Bmatrix} 1/A_w, & \text{for } \mathbf{x} \text{ inside the WS cell} \\ 0, & \text{for } \mathbf{x} \text{ outside the WS cell} \end{Bmatrix}. \tag{5}$$

Figure 1 shows WS cells for square and hexagonal sampling lattices. The Fourier transforms of the pixel function and the WS function are $P(\mathbf{f})$ and $W(\mathbf{f})$, respectively, where $\mathbf{f}$ is a 2-D spatial frequency vector. Analogous with Eq. (3), we express the sampling-and-averaging MTF as the product of these two transforms:

$$\mathrm{MTF}(\mathbf{f})_{\mathrm{total}} \equiv \mathrm{MTF}(\mathbf{f})_{\mathrm{pixel}} \times \mathrm{MTF}(\mathbf{f})_{\mathrm{samp}} = P(\mathbf{f}) \times W(\mathbf{f}). \tag{6}$$

For a given distance $\Delta$ between the samples, $A_w$ for the hexagonal case is smaller than for the square case by factor of $\sqrt{3}/2$. This implies that the MTF of the hexagonal lattice is better than the MTF of the square lattice, which corroborates a previously derived result.[2]

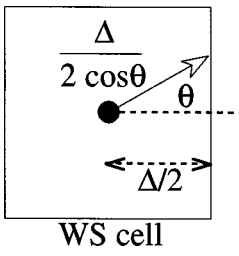


**Fig. 2** Derivation of $\Delta_\theta$ from a WS cell for a square lattice.

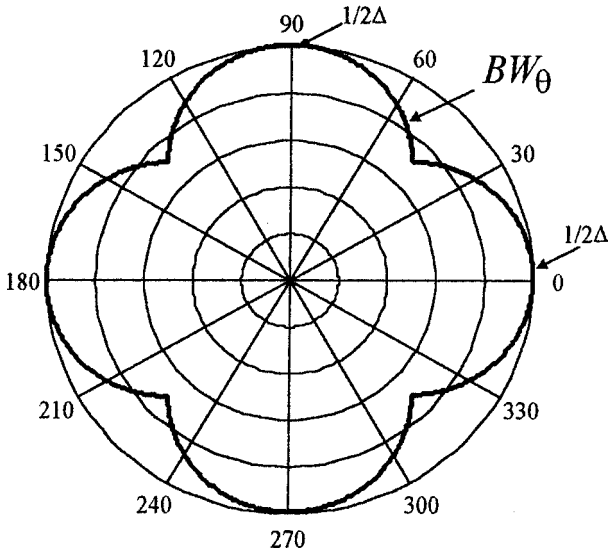


**Fig. 3** BW cell $\mathrm{BW}_\theta$ for a square sampling lattice.

## 3 Bandwidth Cell

We now describe the spatial-frequency-domain figure of merit for the sampling process, the bandwidth cell, which is a Fourier transformation of the WS cell in the spatial domain. Figure 2 shows the relationship of the bandwidth cell for a rectangular lattice according to the distance between the center point of the WS cell and its edge points. This distance $\Delta_\theta$ depends on the angle $\theta$ relative to the horizontal axis as

$$\Delta_\theta = \frac{\Delta}{\cos\theta}, \tag{7}$$

and represents the minimum distance between samples in any given direction. The distance $\Delta_\theta$ is smallest for the horizontal and the vertical directions, in which there is a minimum distance $\Delta$ between lattice points. In all other directions, the distance between adjacent lattice points is longer than the minimum value. Using Eq. (7), it is possible to denote the sampling MTF at a given angle as

$$\mathrm{MTF}(\xi_\theta)_{\mathrm{samp}} = \mathrm{sinc}(\xi_\theta \Delta_\theta). \tag{8}$$

The reciprocal of $\Delta_\theta$ is the location of the first zero of the sinc function, which represents the equivalent-square spatial-frequency bandwidth $\mathrm{BW}_\theta$ of the sampling process in each direction

$$\mathrm{BW}_\theta \equiv \frac{1}{\Delta_\theta} = \frac{\cos\theta}{\Delta}. \tag{9}$$

This function is seen in Figs. 3 and 4 for square and hexagonal lattices, respectively. For a square lattice, $\mathrm{BW}_\theta$ is principally defined over $-45\,\mathrm{deg} < \theta < 45\,\mathrm{deg}$, while for the hexagonal lattice, $\mathrm{BW}_\theta$ is principally defined over $-30\,\mathrm{deg} < \theta < 30\,\mathrm{deg}$.

Let us define an aggregate image-quality figure of merit, the BW area (BWA) as the area encircled by the $\mathrm{BW}_\theta$ function over the angular region $0\,\mathrm{deg} < \theta < 360\,\mathrm{deg}$, repre-

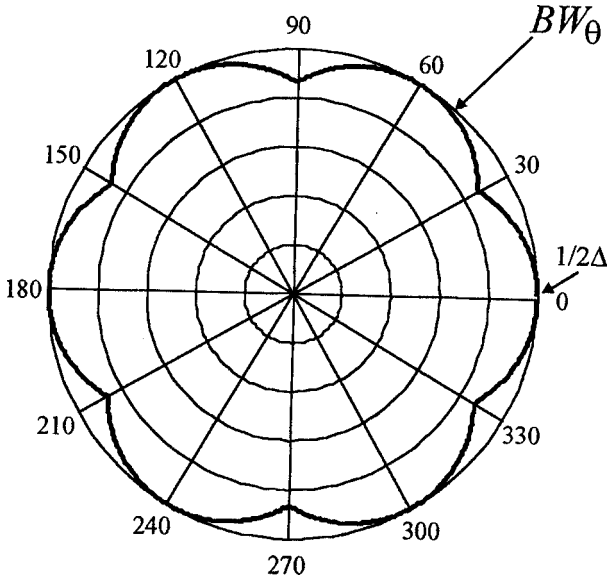


**Fig. 4** BW cell $BW_\theta$ for a hexagonal sampling lattice.

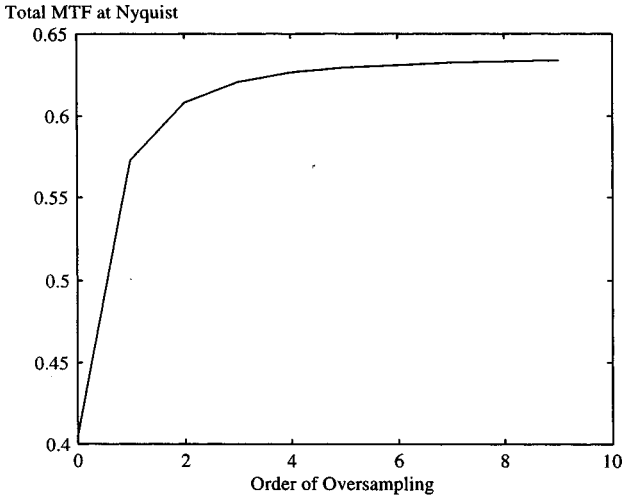


**Fig. 5** Total MTF at the Nyquist frequency as a function of the order of oversampling $n$ for a 1-D contiguous array of square pixels.

senting the 2-D spatial-frequency bandwidth of the sampling process. Using Eq. (9), we can express BWA as

$$\mathrm{BWA}=\left[\frac{\pi}{2}+\frac{\pi}{4}\frac{\sin(2\theta_{\max})}{\theta_{\max}}\right], \tag{10}$$

where $\theta_{\max}=45\,\mathrm{deg}$ for the square lattice and $\theta_{\max}=30\,\mathrm{deg}$ for the hexagonal lattice. This yields

$$\mathrm{BWA}_{\mathrm{square}}=\left(\frac{\pi}{2}+1\right)=2.57, \tag{11}$$

and

$$\mathrm{BWA}_{\mathrm{hex}}=\left(\frac{\pi}{2}+\frac{3\sqrt{3}}{4}\right)=2.87. \tag{12}$$

The ratio between these two bandwidth areas $\mathrm{BWA}_{\mathrm{hex}}/\mathrm{BWA}_{\mathrm{square}}=1.12$, which verifies the bandwidth advantage[4] of 12% of the hexagonal lattice over the square lattice.

## 4 Image-Quality Improvement by Oversampling

The oversampling process can be described as follows. An image irradiance in watts per square centimeter falls on, and is sampled by, an array of pixels. This sampled information is first recorded, then the image is shifted by a fraction of the pixel pitch and resampled.[6–9] The information from the second sample is interlaced with that from the first sample to produce an oversampled image. This process can be repeated as many times as desired. The order of oversampling $n$ is defined as the number of extra samples taken. For instance, order 4 means that the array is shifted consecutively four times by a distance of $p/5$ to obtain four extra samples, giving a total of five samples. Using the total MTF at the spatial Nyquist frequency of the array ($\xi_{\mathrm{Ny}}=1/2\Delta$) as the figure of merit, we investigate the amount of improvement that can be obtained by oversampling an array of contiguous 1-D ($p=\Delta$) pixels. Using Eq. (3), we find

$$\mathrm{MTF}_{\mathrm{total}}(\xi_{\mathrm{Ny}})=\mathrm{sinc}\,(1/2)\times\mathrm{sinc}\,(1/2n). \tag{13}$$

A graph of $\mathrm{MTF}_{\mathrm{total}}$ at the Nyquist frequency as a function of the order of oversampling $n$ is shown in Fig. 5. It is clear that the greatest improvement in image quality is obtained when $n$ is changed from zero to first order. The amount of improvement falls off rapidly for $n>1$. A similar analysis can be applied to a 2-D pixel array, including the angular dependence of the WS cell [Eq. (8)]. We calculate the value of $\mathrm{MTF}_{\mathrm{total}}$ at $\xi_{\mathrm{Ny}}$, averaged over all angles $\theta$. We investigated three types of oversampling geometries for square contiguous pixel arrays: horizontal oversampling only [Fig. 6(a)], both horizontal and vertical oversampling [Fig. 6(b)], and oversampling along the diagonal axis [Fig. 6(c)]. In each configuration the array is shifted by a distance of $p/n$ consecutively $n-1$ times along the sampling direction. A graph of the angle averaged $\overline{\mathrm{MTF}_{\mathrm{total}}(\xi_{\mathrm{Ny}})}$ as a function of $n$ is shown in Fig. 7. The optimum oversampling geometry is to shift with position increments along the diagonal axis, because there are more sampling points per unit area along the 45 deg diagonal axis. Sampling along the diagonal axis with an interval size of $p/n$ is equivalent to sampling at both horizontal and vertical directions with a smaller interval size of $p/(n\sqrt{2})$. It can be shown that the WS cell area

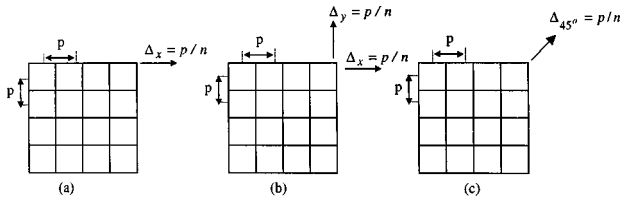


**Fig. 6** Three different oversampling geometries for oversampling: along (a) the horizontal direction, (b) the horizontal and vertical directions, and (c) the 45 deg diagonal axis.

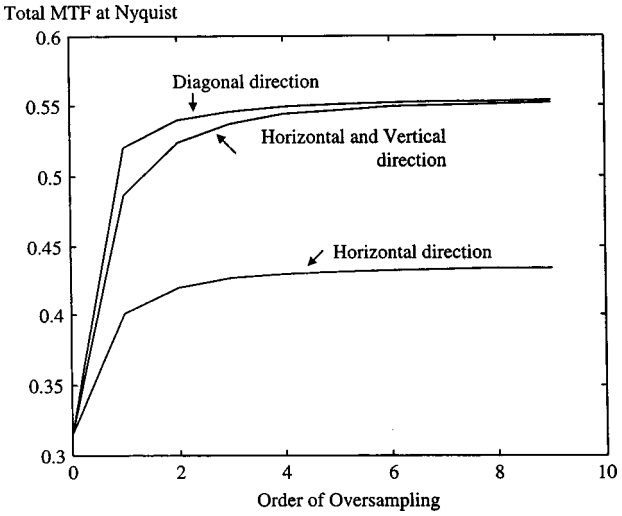


**Fig. 7** Angle-averaged total MTF at the Nyquist frequency as a function of the order of oversampling $n$ for a contiguous 2-D array of square pixels, for three different oversampling geometries.

$A_w$ that arises from sampling along the diagonal axis [Fig. 8(c)] is smaller than for sampling along the horizontal and vertical directions [Fig. 8(b)] by factor of 2, and by factor of $2n$ from the case of sampling only along the horizontal direction [Fig. 8(a)]. This agrees with the results for $\mathrm{MTF}_{\mathrm{total}}(\xi_{\mathrm{Ny}})$ in Fig. 7. Similar results can be shown also for the hexagonal pixel array, while in this case, the optimum sampling direction is at $\theta = 30$ deg. As in the 1-D cases, the greatest improvement for all 2-D cases is obtained when going from $n=0$ to $n=1$.

## 5 Conclusions

A new quantitative metric for describing 2-D sampling was introduced. This metric, the BW cell in the spatial-frequency domain, is the area bounded by the Fourier transform of the WS cell in the spatial domain. The BW cell enables the comparison of different sampling lattice geometries. According to this measure, the hexagonal lattice performance in the sense of average BW is superior to the square lattice by 12%. Three different configurations of the 2-D sampling process were considered. The optimum oversampling geometry was found to be that of shifting the pixel array along the 45 deg diagonal axis for a square pixel array and along the 30 deg for a hexagonal pixel array. The largest amount of improvement occurs along the direction of the poorest initial MTF.

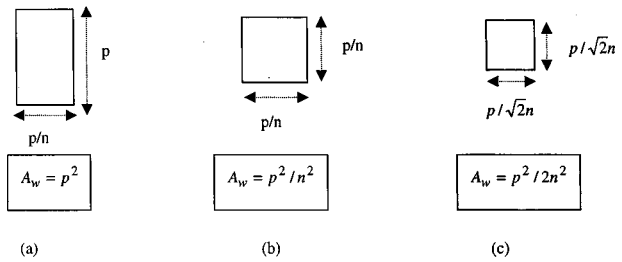


**Fig. 8** WS cell for oversampling along (a) the horizontal direction, (b) the horizontal and vertical directions, and (c) the 45 deg diagonal axis.

### *Acknowledgment*

This work was supported by the Hewlett-Packard University Grants Program and the Clore Foundation, Israel.

### *References*

1. S. K. Park, R. Schowengerdt, and M. A. Kaczynski, ''Modulation-transfer-function analysis for sampled-image systems,'' *Appl. Opt.* **23**, 2572–2582 (1984).
2. K. J. Barnard and G. D. Boreman, ''Modulation transfer function of hexagonal staring focal plane arrays,'' *Opt. Eng.* **30**, 1915–1919 (1991).
3. G. Boreman and A. Plogstedt, ''Spatial filtering by a line-scanned nonrectangular detector application to SPRITE readout MTF,'' *Appl. Opt.* **28**, 1165–1168 (1989).
4. O. Hadar, A. Dogariu, and G. D. Boreman, ''Angular dependence of sampling MTF,'' *Appl. Opt.* **36**, 7210–7216 (1997).
5. N. Ashcroft and N. Mermin, *Solid State Physics*, pp. 63–83, Saunders College, Philadelphia (1976).
6. K. M. Hock, ''Effect of oversampling in pixel arrays,'' *Opt. Eng.* **34**, 1281–1288 (1995).
7. L. deLuca and G. Cardone, ''Modulation transfer function cascade model for a sampled IR imaging system,'' *Appl. Opt.* **13**, 1659–1664 (1991).
8. K. J. Barnard and E. A. Watson, ''Effects of image noise on submicroscan interpolation,'' *Opt. Eng.* **34**, 3165–3173 (1995).
9. K. J. Barnard, E. A. Watson, and P. F. McManamon, ''Nonmechanical microscanning using optical space-fed phased arrays,'' *Opt. Eng.* **33**, 3063–3071 (1994).

**Ofer Hadar** received the BSc, the MSc (cum laude) and the PhD degrees from the Ben-Gurion University of the Negev, Israel, in 1990, 1992, and 1997, respectively, all in electrical and computer engineering. His PhD studies were supported by the Clore Fellowship. His PhD dissertation dealt with the effects of vibrations and motion on image quality and target acquisition. From August 1996 to February 1997, he was with CREOL at Central Florida University, Orlando, Florida, as a research visiting scientist, working on angular dependence of sampling MTF and over-sampling MTF. From October 1997 to March 1999, he was post-doctoral fellow in the Department of Computer Science at the Technion-Israel Institute of Technology. Currently he is a faculty member in the Communication System Engineering Department at Ben-Gurion University of the Negev. His research interests include: image compression, routing in ATM networks, packet video, transmission of video over ATM networks, and, video rate smoothing. Dr. Hadar is a member of SPIE.

**Glenn D. Boreman** is a professor of optics and electrical engineering in the Center for Research and Education in Optics and Lasers at the University of Central Florida. He received a BS in optics from University of Rochester and a PhD in optics from University of Arizona. He has held visiting research positions with the U.S. Army Night Vision Lab, the U.S. Army Redstone Arsenal, Imperial College in London, and the Swiss Federal Institute of Technology in Zurich. Dr. Boreman is the editor of *Applied Optics-Optical Technology*, a past associate editor of *Optical Engineering*, and a member of the SPIE Board of Directors. He is coauthor of *Infrared Detectors and Systems* (Wiley, 1996), author of *Basic Electro-Optics for Electrical Engineers* (SPIE Press, 1998), and editor of *Infrared Technology 1988–1998* (SPIE Press, 1998). He has published more than 70 papers and received the 1995 Kingslake Medal from SPIE.